scientific reports

Check for updates

OPEN

A novel LncRNA risk model for disulfidptosis-related prognosis prediction and response to chemotherapy in acute myeloid leukemia

Yihong Wei[1,2], Hexiao Jia[1,2], Xiaodong Guo[1], Hailei Zhang[1], Xinyu Yang[1], Can Can[1], Na He[1], Hanyang Wu[1], Wancheng Liu[1] & Daoxin Ma[1]✉

Acute myeloid leukemia (AML), the most prevalent acute leukemia in adults, is characterized by its heterogeneity, which contributes to a poor prognosis and high recurrence rate. Recently, a unique form of cell death, called disulfidptosis, has been identified, which could transforming our understanding of and strategy for cancer treatment. Consequently, further inquiry is necessary to explore the possible link between disulfidptosis and AML. To facilitate this analysis, the researchers obtained single-cell RNA sequencing (scRNA-seq) data from AML patients using the Gene Expression Omnibus (GEO) database. By applying the Cox proportional hazards model and least absolute shrinkage and selection operator (LASSO) regression analysis, we created a signature of disulfidptosis-related long non-coding RNAs (DRLs). This predictive model was established based on six specific DRLs (AC005076.1, AP002807.1, HDAC4-AS1, L3MBTL4-AS1, LINC01694, and THAP9-AS1). The utility of this model in forecasting the prognosis of AML patients was corroborated by the receiver operating characteristic (ROC) curve. Moreover, significant variations in the biological functions and signaling pathways were discovered by gene ontology (GO) and Gene Set Enrichment Analysis (GSEA). To further investigate the relationship between immune infiltration, the study assessed variations in immune checkpoint expression and immune cell subset infiltration. Additionally, we used real-time quantitative PCR (RT-qPCR) to detect lncRNA expression in AML and healthy control to substantiate our analysis results. In conclusion, the results of this study may help discover novel therapeutic targets and prognostic biomarkers for AML, paving the way for customized precision chemotherapy.

Keywords Disulfidptosis, Acute myeloid leukemia, LncRNA, Prognostic signature

Abbreviations

AML	Acute myeloid leukemia
DRLs	Disulfidptosis-related long non-coding RNA signature
lncRNAs	Long noncoding RNAs
RCD	Regulated cell death
scRNA-seq	Single-cell RNA-sequencing
PCA	Principal component analysis
DEGs	Differentially expressed genes
TCGA	The Cancer Genome Atlas
DRGs	Disulfidptosis-related genes
ROCs	Receiver operating characteristic curves
AUC	Area under curve
GO	Gene ontology
KEGG	Kyoto encyclopedia of genes and genomes

[1]Department of Hematology, Qilu Hospital of Shandong University, Jinan 250012, Shandong, People's Republic of China. [2]Yihong Wei and Hexiao Jia contributed equally to this work. ✉email: daoxinma@sdu.edu.cn

Acute myeloid leukemia (AML) is a type of hematological malignancy, which is defined by the uncontrollably growing number of immature myeloid cells that fail to undergo normal differentiation. According to predictions by the National Cancer Institute, 20,380 new cases of AML will be recorded in 2023, resulting in approximately 11,310 deaths[1]. Despite recent breakthroughs in AML immunotherapy, including the inhibition of BCL-2, FLT3, isocitrate dehydrogenase (IDH), and Hedgehog signaling pathway, patients with AML continue to face poor outcomes. This is largely due to the uncharted etiologies and complex pathogenesis of AML[2–6]. Therefore, additional research is desperately needed to improve the effectiveness of AML treatments, particularly by focusing on potential therapeutic targets and prognostic biomarkers that could advance individualized precision medicine.

Long noncoding RNAs (lncRNAs), which are noncoding RNA longer than 200 nucleotides without a significant open reading frame, have drawn considerable interest in cancer research[7]. With technological advancements, lncRNA signatures identified through microarrays and RNA sequencing have shown potential in predicting cancer prognosis and therapy outcomes[8,9]. Notably, cancer cells exhibit distinct metabolic processes compared to normal cells, offering new avenues for therapeutic intervations[10]. Regulated cell death (RCD) is an important aspect of metabolic therapy for cancer[11]. Recently, a unique form of cell death, termed disulfidptosis, was recently identified by the Gan laboratory[12]. This form of cell death is caused by high-level expression of SLC7A11 in kidney cancer cells. In particular, under conditions of glucose starvation, these cells experience rapid NADPH depletion, leads to disulfide buildup. This results in disulfidptosis, which is characterized by the formation of disulfide bonds in actin cytoskeleton proteins under disulfide stress. The subsequent collapse of the actin filament network ultimately triggers cell death. While the link between disulfidptosis and malignancy has been established, its specific connection to AML remains unexplored.

In this study, we discovered a novel set of disulfidptosis-related lncRNAs (DRLs), examined its predictive values, and considered its possible effects on the tumor microenvironment in AML. The principal aim of the study was to exhibit the effectiveness of DRLs in evaluating the prognosis of patients with AML and in clarifying possible therapy options.

Materials and methods

Single-cell transcriptome analysis

The scRNA-seq matrix file was downloaded from the GEO (GSE116256) dataset. Seurat (version 4.0.2, R version 4.3.2) was utilized for downstream analysis. Cells were excluded based on the following thresholds: > 2500 or < 500 expressed genes, > 5% mitochondrial content, or > 40 ribosomal gene counts[13]. Highly variable genes were found using Seurat's FindVariableGenes function, and these were subsequently normalized within each cell. Principal component analysis (PCA) was then used on the highly variable genes. The top 20 significant principal components were selected for the t-distributed stochastic neighbor embedding (t-SNE) projection. Differentially expressed genes (DEGs) were identified using Seurat's FindAllMarkers function, and their significance was assessed with the Wilcox test. For the manual annotation of different clusters, the Cellmarker 2.0 website and information from previous studies were used to identify marker genes.

Score according to disulfidptosis-related genes (DRGs)

To calculate the module scores of DRGs in single cells, we utilized Seurat's AddModuleScore function, focusing on 9 DRGs (FLNA, FLNB, MYH9, MYH10, NDUFA11, NDUFS1, NUBPL, SLC7A11, TLN1) that were identified in the previous study.

Gene expression data acquisition

Gene expression and clinical data for 150 AML patients were downloaded from The Cancer Genome Atlas (TCGA) (https://portal.gdc.cancer.gov/) database, and the gene expression data of 337 normal whole-blood samples were retrieved from Genotype-Tissue Expression (GTEx) project database. The association between DRGs and lncRNAs was verified using Pearson correlation analysis with disulfide-related lncRNAs limited to those with a correlation coefficient $|R| > 0.4$ and $p < 0.001$. Sankey diagrams were created using the "limma" and "ggplot2" packages to visualize the results.

Development and validation of a prognostic signature for disulfidptosis-related LncRNAs (DRLs)

The patients in the TCGA database were used to generate randomization in the patient population for the training and validation groups. Univariate Cox regression analysis revealed that lncRNAs associated with disulfidptosis (DRLs) significantly ($p < 0.05$) affect patient prognosis. Subsequently, we employed LASSO-Cox regression for feature selection. The optimal penalty parameter λ was determined through 10-fold cross-validation, and this process was implemented using the glmnet package. Based on the screened genes, a multivariate Cox model was constructed, and the variable combination was further optimized through stepwise regression. Finally, a prognostic risk assessment model was established. The following risk score formula was developed for each AML patient:

$$\begin{aligned}\mathrm{DRLs} = {} & (\mathrm{coefAC005076.1} \times \mathrm{expAC005076.1}) + (\mathrm{coefAP002807.1} \times \mathrm{expAP002807.1}) \\ & + (\mathrm{coefHDAC4-AS1} \times \mathrm{expHDAC4-AS1}) + (\mathrm{coefL3MBTL4-AS1} \times \mathrm{expL3MBTL4-AS1}) \\ & + (\mathrm{coefLINC01694} \times \mathrm{expLINC01694}) + (\mathrm{coefTHAP9-AS1} \times \mathrm{expTHAP9-AS1}),\end{aligned}$$

Here, coeflncRNA represents the correlation between lncRNA and patients survival, and explncRNA represents the expression level of each lncRNA. Using this formula, each patient in the TCGA database was assigned a risk score, allowing classification into low- and high-risk categories.

Survival analysis
Kaplan-Meier (K-M) survival analysis was conducted using the "survival" and "survminer" R packages. The log-rank test evaluated survival curve differences. Training, testing, and TCGA cohorts were automatically partitioned via the createDataPartition function in the "caret" package, without applying multiple testing corrections (e.g., FDR). Additionally, survival analysis was extended to patients with varying clinical traits. The "timeROC" R package was utilized to analyze the 1-, 3-, and 5-year receiver operating characteristic curves (ROCs), which evaluate the predicted effectiveness of the lncRNA prognostic model.

Independent prognostic analysis
Clinical factors such as age, gender, cytogenetic risk, FAB subtype, FLT3 mutant and risk score of our model were used to analyze the relationship between survival. Gender (male/female) and FLT3 mutation status (mutated/unmutated) were treated as categorical variables, while age (years), FAB subtype, and Cytogenetic Risk were analyzed as continuous variables. Then, univariate and multivariate Cox regression analyses were carried out using the "limma" R package to find independent prognostic factors among these variables.

Principal component analysis (PCA) and nomogram
The "limma" program was used to perform PCA to compare the distribution of disulfidptosis-related lncRNAs between the low- and high-risk groups. To develop a nomogram for AML patients, the "regplot" R package was utilized, incorporating clinical characteristics such as age, gender, and risk score, to predict survival rate.

Gene ontology (GO) analysis and the gene set enrichment analysis (GSEA)
With a screening condition of p-value < 0.05 and Log2 (Fold Change) |>1|, GO analysis was conducted by using the "clusterProfiler" R package. Furthermore, pathways in both high- and low-risk groups were found by using Gene Set Enrichment Analysis (GSEA). The analysis utilized the Molecular Signatures Database (MSigDB) C2 curated gene set collection (c2.cp.kegg.Hs.symbols.gmt).

Immune micro-environment evaluation
The ESTIMATE package was utilized to estimate stromal, immune, and ESTIMATE scores for the two groups[14]. The percent of immune cell infiltration was determined using the CIBERSORT algorithm[15]. Additionally, single-sample gene set enrichment analysis (ssGSEA) was performed to assess immune-related functions in both low- and high-risk populations[16]. Immune checkpoint molecules were visualized using the "ggplot2" R package.

Drug sensitivity
The half-maximal inhibitory concentrations (IC50) of commonly used anticancer medicines were computed using the "oncoPredict" R package. This enable the assessment of potential efficacy of targeted treatment medicines or chemotherapy in different risk groups.

RNA extraction
Bone marrow samples were collected from 4 healthy individuals and 5 newly diagnosed AML patients. Trizol was used to extract total RNA for following experiments.

Real-time quantitative PCR (RT-qPCR)
The Prime Script RT reagent Kit Perfect Real Time (Takara Bio, Japan) was applied to reverse transcribe the total RNA into cDNA. RT-qPCR analysis was conducted using the LightCycler 480II real-time PCR system (Roche, Switzerland). Primers used in the RT-qPCR, provided by BioSune Company (China), were as follows:

AC005076.1-130 (homo) forward: GCA GCC GTA TAA ACC CAT CC, reverse: CTT TGG TTC CTG TCA CAT ACG C; GAPDH (homo) forward: GCA CCG TCA AGG CTG AGA AC, reverse: TGG TGA AGA CGC CAG TGG A. The expression of lncRNA was determined by using the $2^{-\Delta\Delta T}$ method.

Small interfering RNA (siRNA) experiments
AC005076.1 siRNA and negative control were obtained from BioSune Company (China). THP-1 and MOLM-13 cells were cultured in 6-well plates and transfected with siRNA using Lipofectamine 2000 (Invitrogen) in serum-free medium for 6 h, after which complete medium was added. Subsequent experiments were performed 48 h post-transfection. The sequences of the siRNAs are as follows: sense: S: GUC GUU CUU GAU GAA AUG UTT; AS: ACA UUU CAU CAA GAA CGA CTT. The sequences for the negative control siRNA were: sense: UUC UCC GAA CGU GUC ACG UTT; anti-sense: ACG UGA CAC GUU CGG AGA ATT.

Statistics analysis
GraphPad 8.0 was used to analyze the data, which were presented as mean ± SEM. A Student's t-test (two-tailed) was used to examine the data between the groups. P values are indicated as $*P < 0.05$.

Results
Differential expression of DRGs and identification of DRLs in AML
The flow diagram depicting the study is shown in Fig. 1. Firstly, to confirm the influence of DRGs in AML, we utilized single-cell transcriptomic analyses to explore the relationship between DRGs and AML. Analysis of

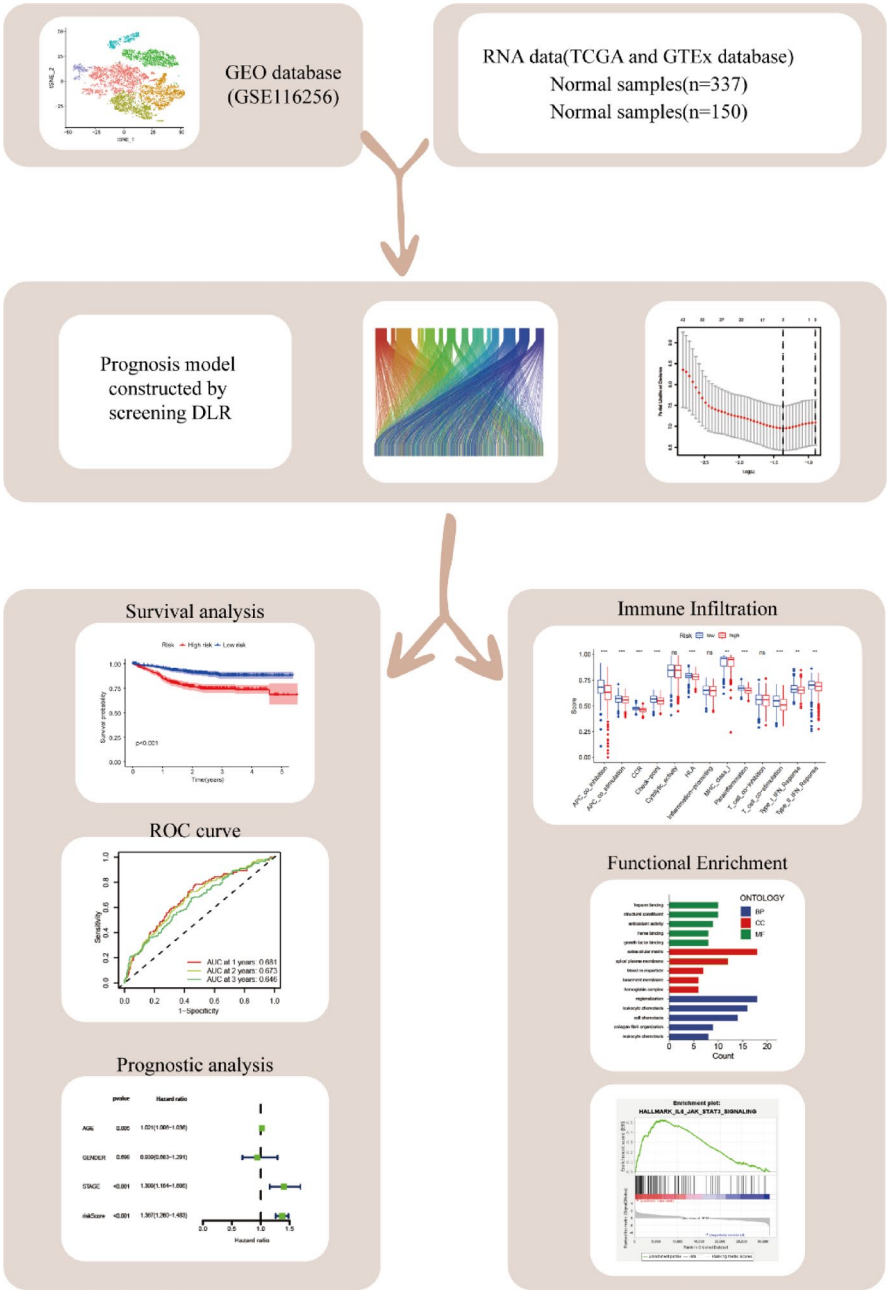

Fig. 1. The flowchart of our study.

the scRNA-seq data from the GEO database (GSE116256) confirmed the presence of DRGs in AML patients. Following stringent filtration, 20,378 single cells from 16 newly diagnosed AML patients and 5 healthy controls were categorized into 13 distinct clusters (Fig. 2A,B). The identification of each cluster was validated by annotating the cells with commonly recognized markers (Fig. 2C). Clusters containing a high proportion (>70%) of cells from healthy controls were classified normal-like cells, while the remaining clusters were identified as malignant-like cells. Consequently, Clusters 0, 1, 2, 4, 6, 8 and 10 were classified as malignant cells (Fig. 2B). We employed the AddModuleScore function (Seurat) package to assess the expression levels of 9 DRGs: FLNA, FLNB, MYH9, MYH10, NDUFA11, NDUFS1, NUBPL, SLC7A11, and TLN1. The analysis revealed that DRGs were expressed at significantly higher levels in malignant cells compared to normal cells (Fig. 2D). These results indicate that DRGs are essential for the development of AML. Given the pivotal role of lncRNAs in gene expression regulation, we further investigated lncRNAs associated with disulfidptosis. Through Pearson correlation analysis, we screened for disulfidptosis-related lncRNAs and identified 326 disulfidptosis-related lncRNAs (Fig. 2E,F).

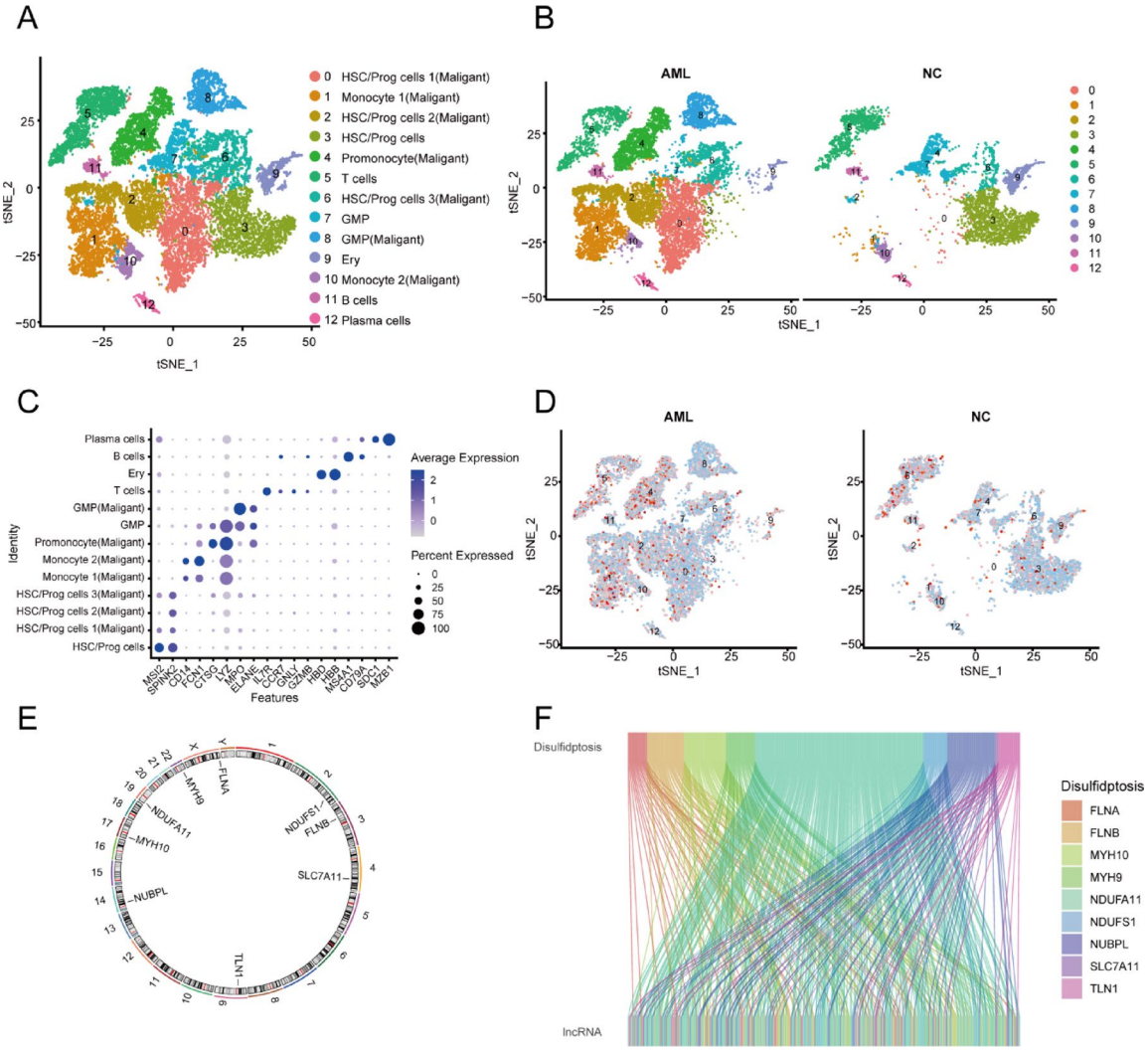

Fig. 2. The identification of disulfidptosis-related lncRNAs. (**A**) T-distributed stochastic neighbor embedding (t-SNE) plots of AML and health control, which included HSC/Prog cells (Malignant/Normal), Monocyte (Malignant), Promonocyte (Malignant), GMP (Malignant/Normal), T cells, CTLs, erythroid cells, B cells, and Plasma cells. (**B**) t-SNE plots of AML and health patients. t-SNE plot of AML patients was on the left panel, and health control was on the right panel. (**C**) Cluster-specific marker genes of each cluster were depicted in a dot plot, with color and size indicating effect size. (**D**) t-SNE plots displayed expression scores of DRGs in AML and healthy control cells. Color gradation represented score levels. (**E**) The location of DRGs on the chromosomes. (**F**) The Sankey diagram of the lncRNAs co-expressed with disulfidptosis-related genes.

Development and verification of a risk model derived from DLRs

First, univariate Cox regression analysis identified 38 lncRNAs from a total of 299 lncRNAs that were significantly associated with AML prognosis (Fig. 3A). This list was subsequently refined using the LASSO approach (Fig. 3B). Through the construction of a cross-validated model and analysis of changes in regression coefficients, six lncRNAs were identified as being relevant to AML prognosis (Fig. 3C). Based on these six lncRNAs, a risk-scoring model was constructed. The coefficients for each lncRNA are shown in Table 1. The risk score was calculated using the following equation:

$$\begin{aligned}\text{Risk score} = {} & (\text{coefAC005076.1} \times \text{expAC005076.1}) + (\text{coefAP002807.1} \times \text{expAP002807.1}) \\ & + (\text{coefHDAC4} - \text{AS1} \times \text{expHDAC4} - \text{AS1}) + (\text{coefL3MBTL4} - \text{AS1} \times \text{expL3MBTL4} - \text{AS1}) \\ & + (\text{coefLINC01694} \times \text{expLINC01694}) + (\text{coefTHAP9} - \text{AS1} \times \text{expTHAP9} - \text{AS1}).\end{aligned}$$

In addition, a heatmap (Fig. 3D) was generated to show the associations between the six predictive lncRNAs and disulfidptosis-associated genes.

Using the above equation, the risk score was calculated for each patients in the TCGA cohort. Patients were then randomly divided into training and verification cohorts. Based on the median risk score, patients were split into high-risk ($n = 76$) and low-risk ($n = 65$) cohorts (Fig. 4A–F). Kaplan–Meier survival analysis indicated that

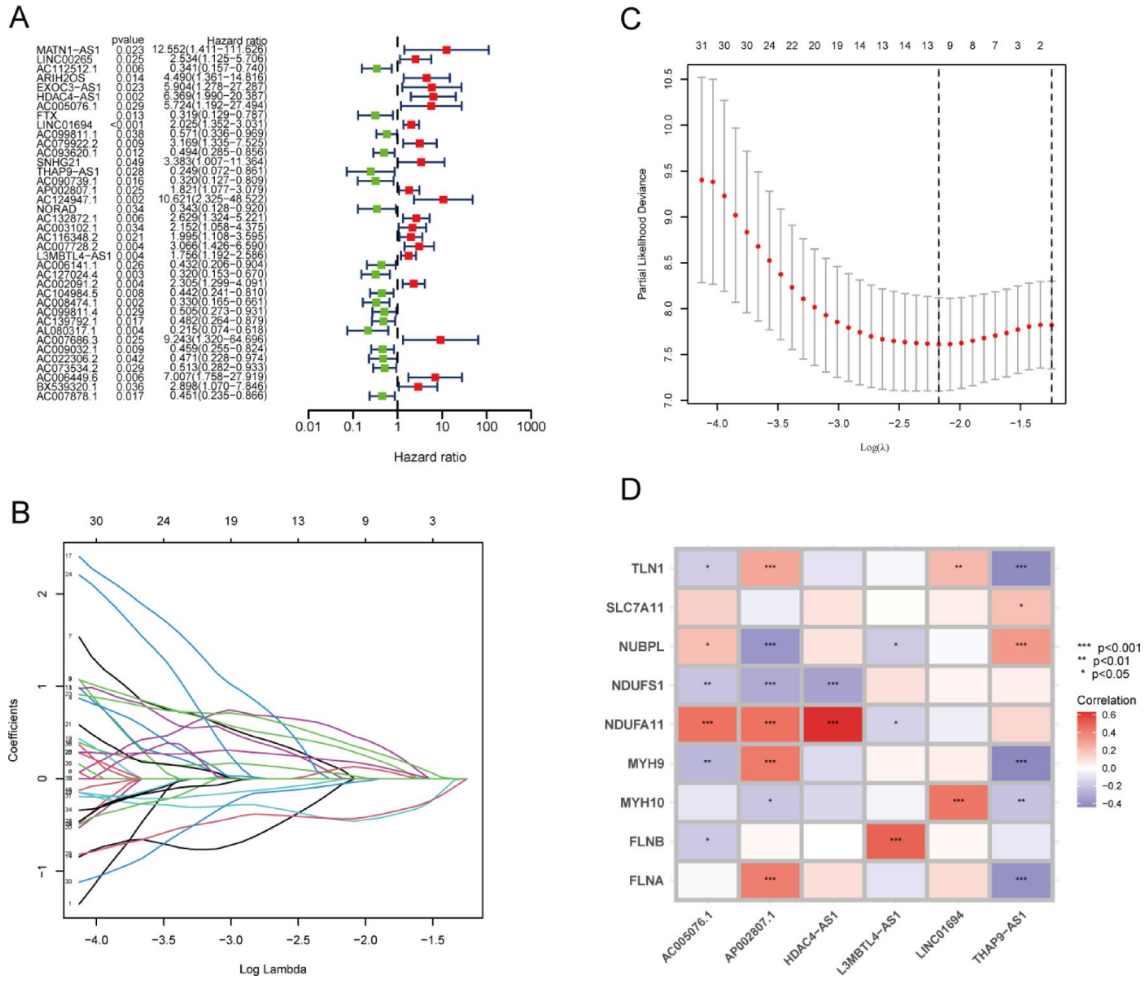

Fig. 3. Construction of DRLs model in AML. (**A**) A forest plot showed the 38 disulfidptosis-related lncRNAs associated with prognosis through a Univariate Cox regression analysis. (**B**) Lasso regression coefficients of disulfidptosis-related lncRNAs. (**C**) Lasso coefficient curve. (**D**) The heatmap showed the correlation between 9 disulfidptosis-related genes and 6 disulfidptosis-related lncRNAs.

Gene	Coefficient
AC005076.1	1.88699969301826
HDAC4-AS1	1.62883321657312
LINC01694	0.906672021732108
THAP9-AS1	−2.04352148844543
AP002807.1	0.593888909378619
L3MBTL4-AS1	1.04456945449904

Table 1. The coefficient of disulfidptosis-related LncRNAs.

the low-risk group had a significantly longer overall survival (OS) than the high-risk group (Fig. 4J–L). Certain lncRNAs, such as HDAC4-AS1, AC005076.1, LINC01694, AP002807.1, and L3MBTL4-AS1, were predominantly upregulated in the high-risk group, according to the heatmap, whereas THAP9-AS1 was primarily upregulated in the low-risk group (Fig. 4G–I).

Evaluation of the clinical predictive ability of the DRLs

Given the accuracy of our model in survival analysis, we further explored whether our risk model could serve as an independent prognostic factor, distinct from other clinical characteristics. We incorporated patients' sex, age, cytogenetic risk, FAB subtype, FLT3 mutation and risk classification into univariate and multivariate Cox regression analyses. The analytic results revealed that the predictive power of DRLs remained independent of other clinical features (Fig. 5A,B). The areas under the ROC curves (AUCs) for 1-, 3-, and 5-year survival were

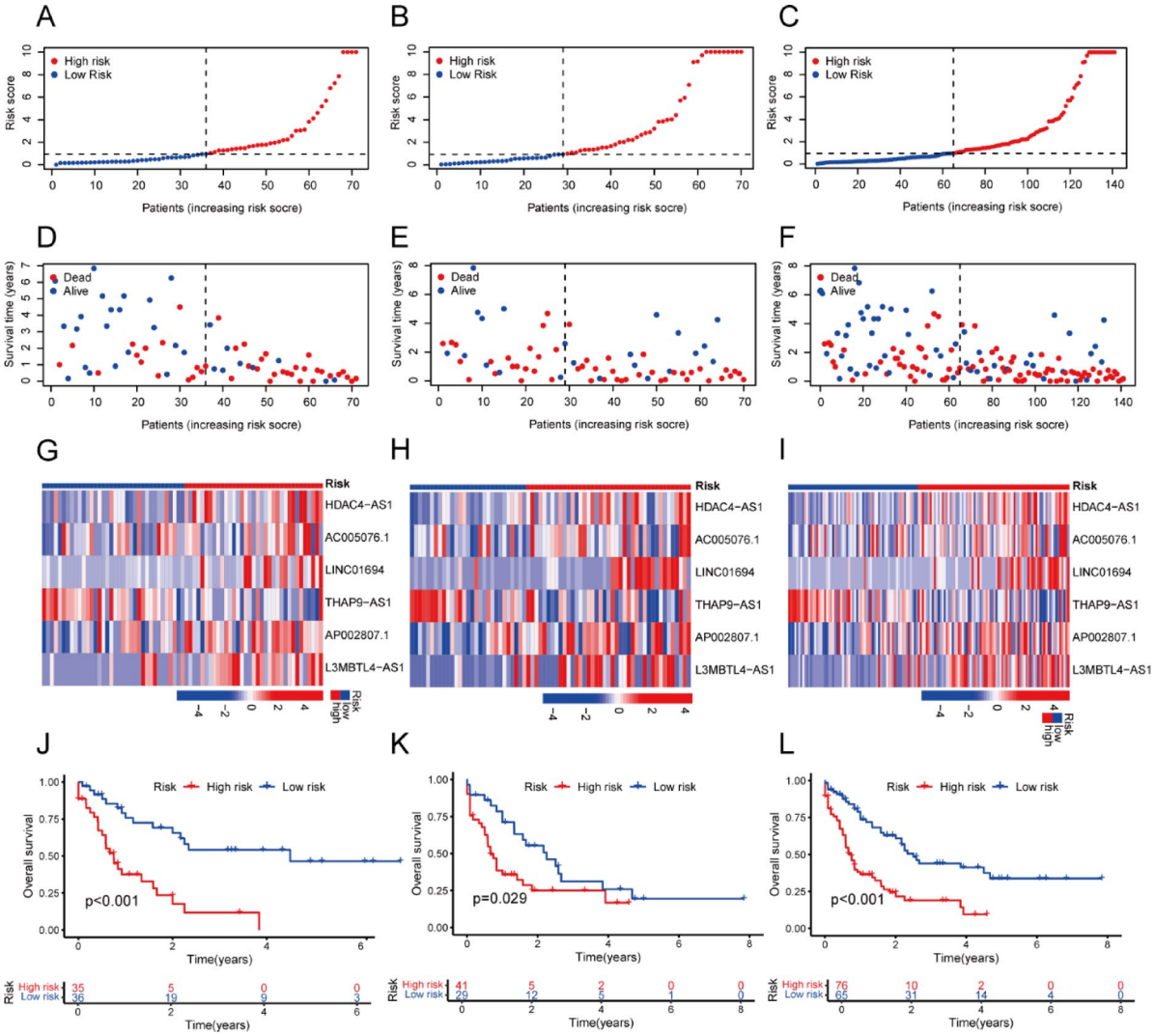

Fig. 4. Evaluation of the risk schema across multiple cohorts. (**A–C**) Distribution of risk quotients in the training, testing, and TCGA cohort. (**D–F**) Mortality statistics across the training, testing, and TCGA cohort. (**G–I**) Heatmaps depicting the 5 lncRNA expression profiles in the training, testing, and TCGA cohort. (**J–L**) Kaplan-Meier survival plots for subjects belonging to high- and low-risk categories in the training, testing, and TCGA cohort.

0.809, 0.705, and 0.874, respectively (Fig. 5C), indicating the high prognostic accuracy of DRLs. Additionally, the AUC of DRLs indicated that the DRL-based model had greater sensitivity and specificity than other prognostic factors, such as sex, FAB subtype, and cytogenetic risk (Fig. 5D). Moreover, to further validate our findings, we collected bone marrow cells from five AML patients and four healthy individuals. The gene AC005076.1, which had the highest weight in the risk score formula, was selected for expression analysis. The results were consistent with our previous bioinformatics analysis (Fig. 5E). Furthermore, a nomogram incorporating sex, age, and the risk score was developed to predict the 1-, 3-, and 5-year survival rate of patients. The calibration diagram revealed that the nomogram has strong predictive ability (Fig. 5F,G). Moreover, analysis of the survival curves revealed that the prognostic model was applicable across a range of clinical subgroups (Fig. 5H–J). Collectively, these results underscore the robust predictive ability of the DRL-based prognostic signature.

PCA and gene enrichment analysis

To obtain a more detailed understanding of the biological processes and networks associated with the identified risk factors, differential expression analysis was performed to identify DEGs between risk subgroups. GO enrichment analysis revealed that the primary functions of the DEGs related to risk were cytokine binding, collagen-containing extracellular matrix, peptide binding, the external side of the plasma membrane, and positive regulation of cytokine production (Fig. 6A). Additionally, KEGG enrichment analysis revealed that the DEGs in the high-risk category were predominantly involved in the chemokine signaling pathway (Fig. 6B). Similarly, GSEA further confirmed significant enrichment of the chemokine signaling pathway in the high-risk group (Fig. 6C). These findings provide strong evidence supporting the functional involvement of DRLs in AML.

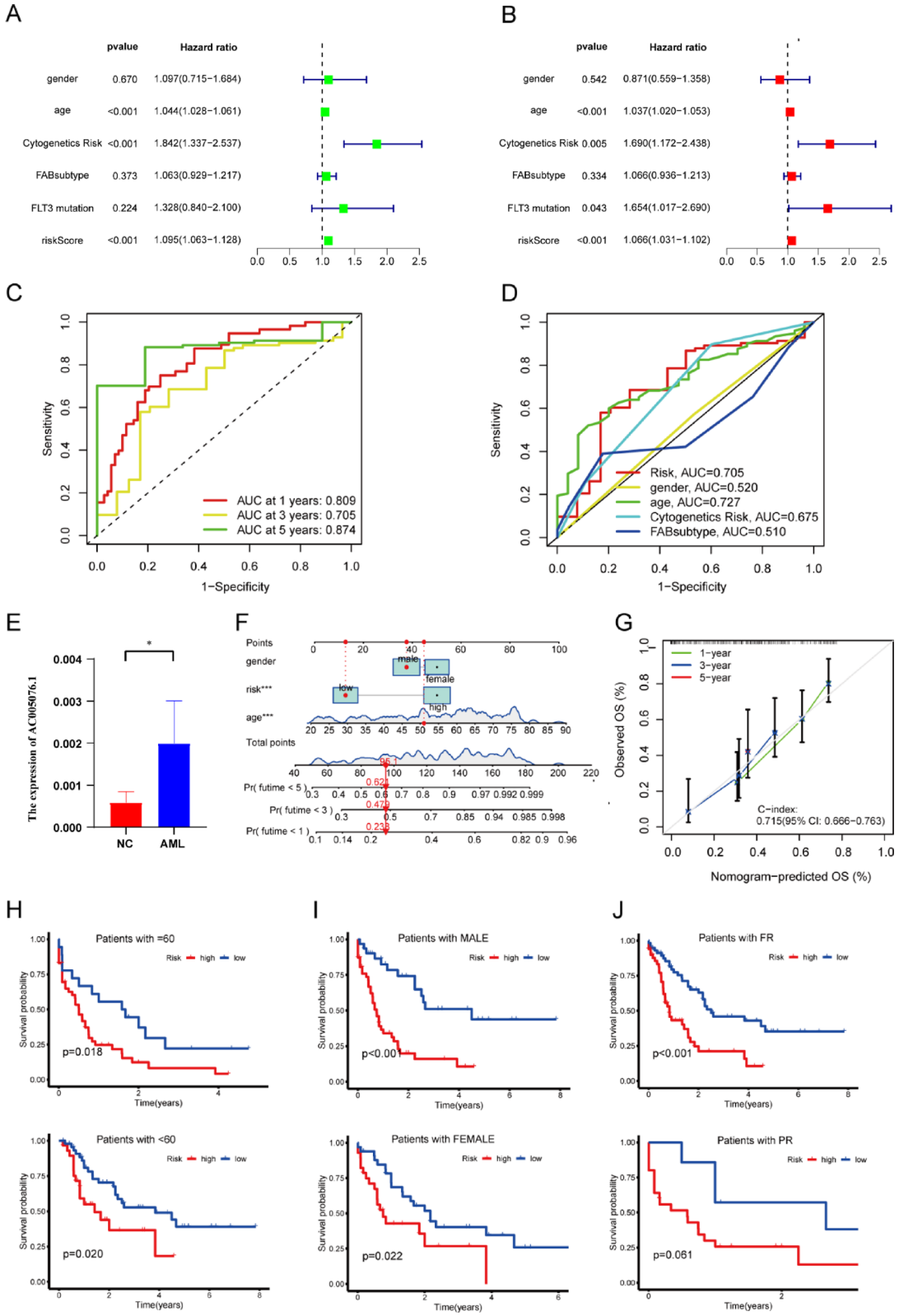

Moreover, our PCA results, based on DRLs, demonstrated that our model has a superior ability to distinguish between the two groups compared to PCA based on disulfidptosis-related mRNAs (Fig. 6D).

Correlation of immune infiltration with the risk score and immunotherapy response

Enrichment analysis revealed that structural components of the extracellular matrix and receptor interactions were differentially enriched between the risk groups. This prompted us to assess the levels of immune cell infiltration in the bone marrow microenvironment of AML patients in the two groups. Using the ESTIMATE algorithm, we found that high-risk patients had higher ESTIMATE and immune scores compared to low-risk

Fig. 5. Validation of the disulfidptosis-related lncRNA signature. (**A, B**) The analysis was conducted involving both univariate and multivariate Cox regression of clinical variables and risk score. (**C**) Full spectrum of ROC curves spanning 1-, 3-, and 5-year timelines. (**D**) ROC diagrams that used to compare the performance of risk scores with clinical variables. (**E**) The expression of AC005076.1 in 5 AML patients and 4 normal control (NC). (**F**) The nomogram predicted the survival rates for AML patients at 1, 3, and 5 years. (**G**) 1-, 3-, and 5-year calibration graphs for the nomogram. (**H–J**) Kaplan-Meier survival plots for the high- and low-risk groups stratified by diverse clinical variables. (**H**) age, upper panel: age ≥ 60; lower panel: age < 60 (**I**) gender, upper panel: male; lower panel: female (**J**) cytogenetic risk, upper panel: FR: favorable risk and intermediate; lower panel: poor risk.

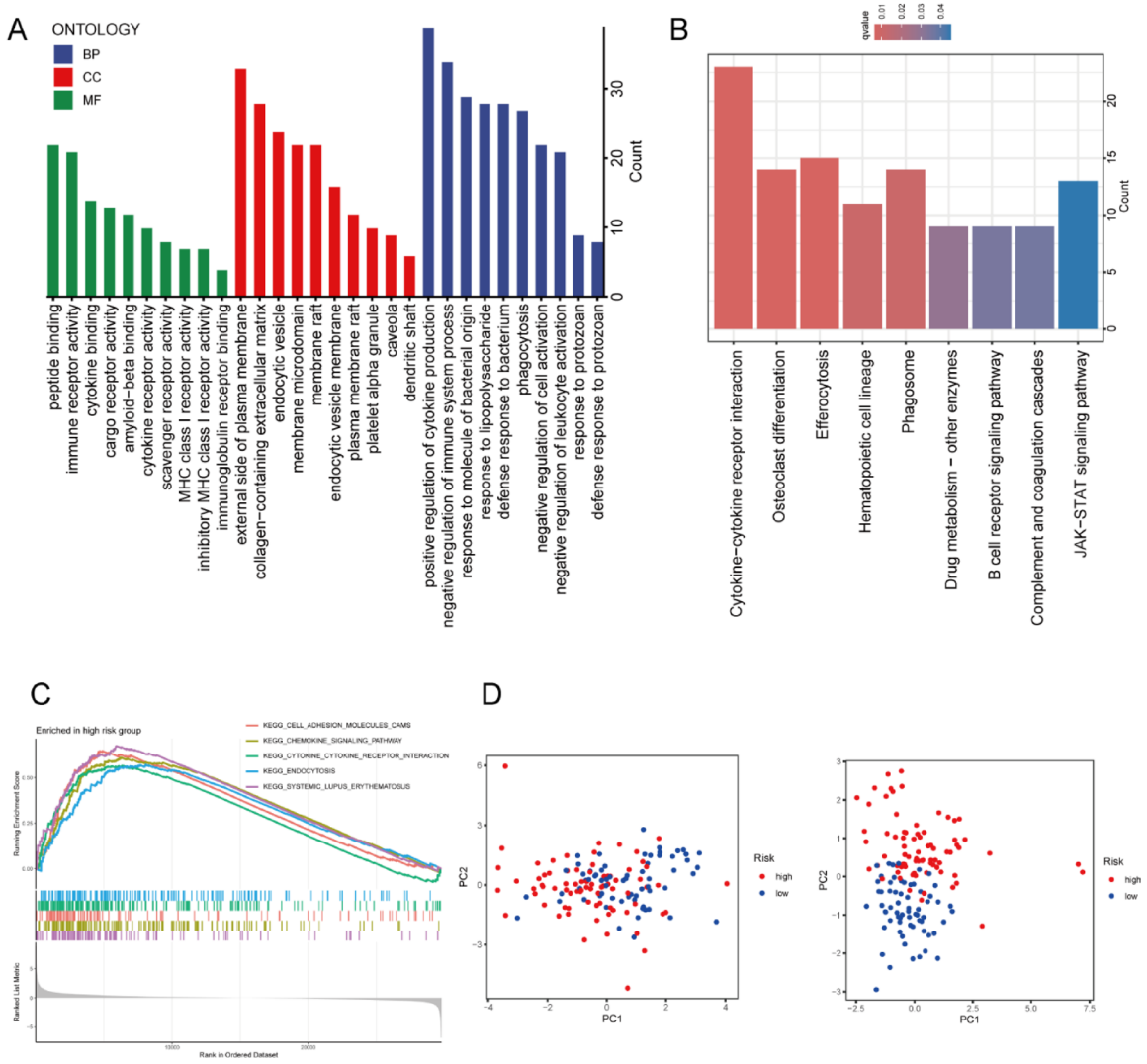

Fig. 6. The functional enrichment analysis and principal component analysis (**A**) GO enrichment analysis was used to determine the cellular component (CC), molecular function (MF), and biological process (BP) pathways of AML patients. (**B**) KEGG pathway enrichment (**C**) GSEA results in high-risk group. (**D**) Principal component analysis (PCA) based on 9 disulfidptosis-related mRNAs (left panel) and 6 disulfidptosis-related lncRNAs (right panel).

patients (Fig. 7A). Additionally, immune cell infiltration in both groups was further validated using several other algorithms, such as CIBERSORT, CIBERSORT-ABS, QUANTISEQ, MCPCOUNTER, XCELL and EPIC (Fig. 7B). The infiltration levels of follicular helper T cells, gamma delta T cells, and resting mast cells were higher in the low-risk group, whereas the high-risk group exhibited significantly greater infiltration levels of T cell regulatory (Tregs) and monocytes (Fig. 7C). Furthermore, the ssGSEA results revealed that immune-related functions were more enriched in the high-risk group (Fig. 7D). Moreover, we also compared the expression levels of immune checkpoint-related genes between the high- and low-risk groups, finding that all immune checkpoint genes were upregulated in the high-risk group (Fig. 7E). This indicated that patients in the high-risk

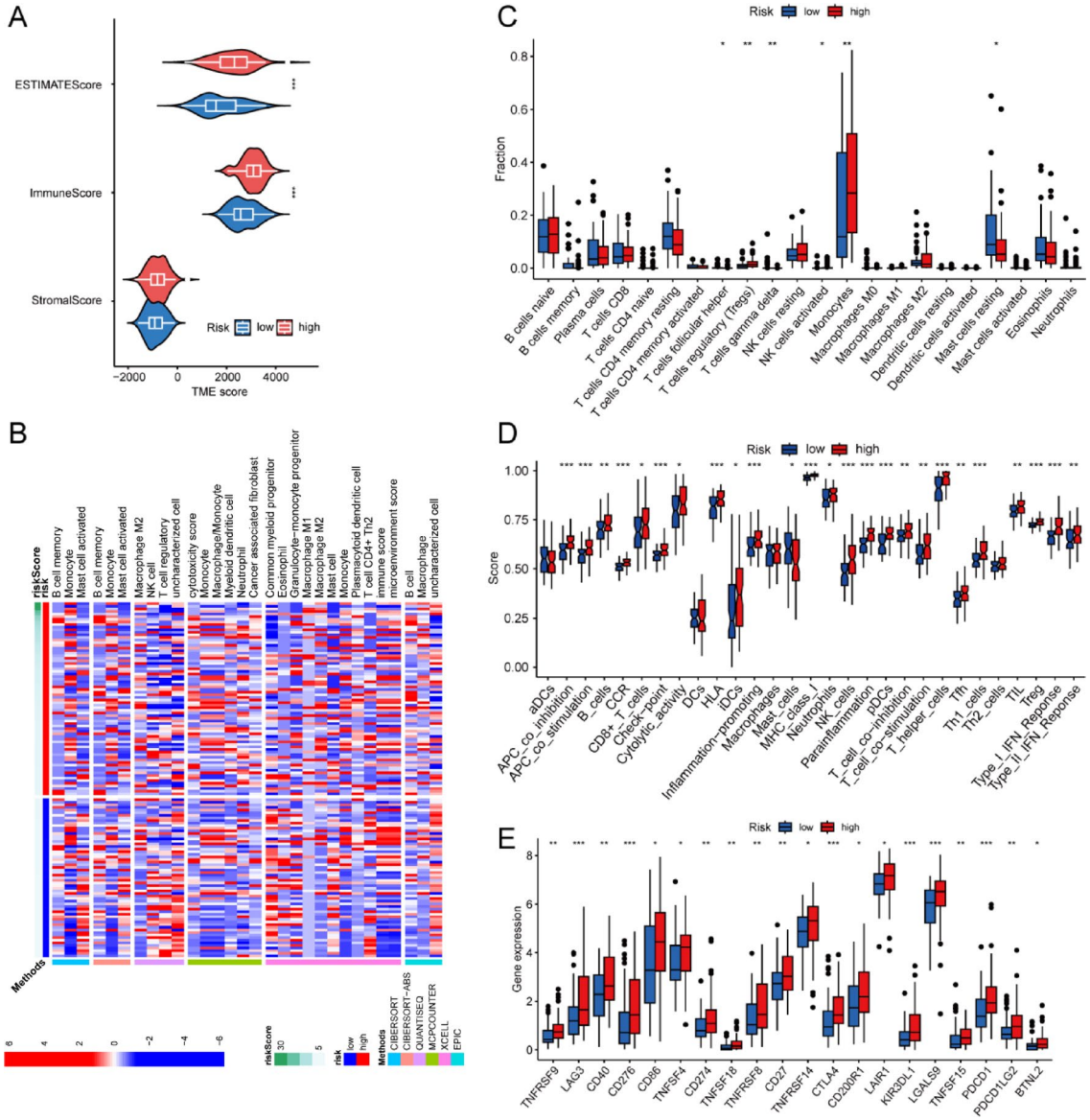

Fig. 7. Immune infiltration analysis. (**A**) ESTIMATE score, Immune score, and Stromal score in the high-, and low-risk groups. (**B**) The proportion of various immune cells in the high-low risk group calculated by CIBERSSORT, CIBERSORT-ABS, QUANTISEQ, MCPCOUNTER, XCELL and EPIC algorithm. (**C**) Immune cell infiltration statistical bar chart speculated by CIBERSORT algorithm in the high- and low-risk group. (**D**) Immune-related functions in the high- and low-risk group. (**E**) Immune checkpoint-related genes in the high- and low-risk group.

group may be more sensitive to immunotherapy. Taken together, these results suggest that the DRL risk score model has the potential to predict immunotherapy response in AML patients.

Analysis of drug sensitivity

Considering the crucial role of chemotherapy and targeted drug therapy in managing AML, it is important to examine differences in drug sensitivity between the risk groups. The "oncoPredict" package was utilized to determine the half-maximal inhibitory concentration (IC50) values of selected drugs (Fig. 8A–H). The high-risk group exhibited increased sensitivity to obatoclax mesylate, venetoclax, and navitoclax drugs that have been reported to show favorable responses in patients with lymphoblastic lymphoma or relapsed/refractory acute lymphoblastic leukemia. Furthermore, samples from the low-risk group exhibited increased sensitivity to the PI3K pathway kinase inhibitor GNE-317 and the vinblastine analog pictilisib, dactolisib, vinblastine, and vinorelbine. Additionally, we used siRNA to downregulate the AC005076.1 to test the response of AML cell to the chemotherapy. Consistent with our analytic result, the finding showed a significant increase in apoptotic AML cells after downregulating AC005076.1 (Supplementary Fig. 1).

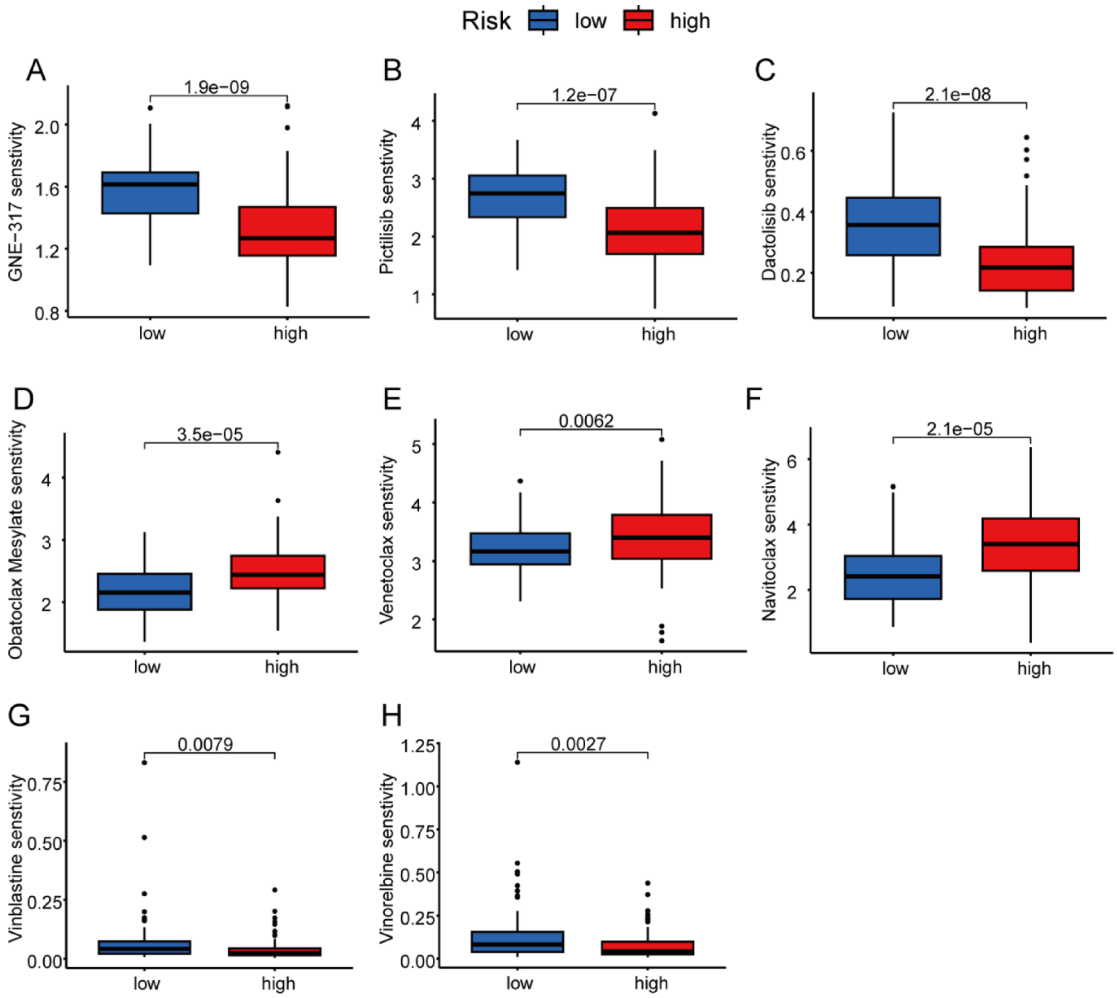

Fig. 8. Drug sensitivity predictions. (**A–H**) GNE-317, pictilisib, dactolisib, obatoclax mesylate, venetoclax, navitoclax, vinblastine, and vinorelbine.

Discussion

AML is a heterogeneous disease that is defined by the unchecked growth of hematopoietic cells[17,18]. Owing to its diverse genetic and molecular abnormalities, the long-term survival and complete remission (CR) rates of AML patients remain unsatisfactory, underscoring the need for novel prognostic markers and therapeutic strategies. The evasion of regulated cell death is a central hallmark of cancer development. Recently, a distinct form of cell death, termed disulfidptosis, has been identified by the Gan laboratory[12], wherein under glucose starvation, high intracellular disulfide levels trigger the collapse of F-actin through disulfide bond formation, leading to cell death. This process is tightly regulated by actin polymerization and Rac GTPase activity, highlighting the cytoskeleton's vulnerability to disulfide stress. In addition, lncRNAs have attracted a lot of focus because of their vital functions in promoting and sustaining tumor initiation and progression[19,20]. Therefore, constructing a lncRNA risk model for AML patients exhibiting disulfidptosis could provide valuable insights into patient outcomes and tumor characteristics.

Our study developed a prognostic risk model for AML patients using six lncRNAs. THAP9-AS1 was mainly expressed in low-risk individuals, while HDAC4-AS1, AC005076.1, LINC01694, AP002807.1, and L3MBTL4-AS1 were highly expressed in high-risk patients. Nomograms, ROC curves, and calibration curves were used to validate the correctness of our model and corroborate the predicted outcomes. The importance of these lncRNAs in cancer prognosis and progression has been shown in earlier research. For instance, THAP9-AS1 has been implicated in multiple solid tumors and shown to promote cell growth and inhibit apoptosis through interactions with miR-484 and YAP signaling[21–24]. HDAC4-AS1 responds to oxygen tension and is involved in redox regulation[25]. LINC01694 regulates the miR-340-5p/SOX4 axis to enhance tumor malignancy[26]. AP002807.1 is associated with autophagy regulation and prognosis in clear cell renal carcinoma[27], while L3MBTL4-AS1 is enriched in CCR2 + macrophages, suggesting immunological functions[28]. AC005076.1 remains largely uncharacterized, highlighting its potential novelty in AML biology.

Building upon existing studies, a deeper functional exploration suggests that these six lncRNAs may regulate critical biological processes associated with AML progression and disulfidptosis susceptibility. Specifically, THAP9-AS1 may modulate cytoskeletal dynamics and oxidative stress responses via miR-484/YAP signaling,

potentially attenuating disulfidptosis[29]. HDAC4-AS1 represses HDAC4 transcription under stress conditions, thereby impairing cytoskeletal stability and sensitizing cells to oxidative damage[30]. LINC01694, by promoting SOX4 expression through miR-340-5p sponging, may facilitate leukemic cell proliferation and resistance to stress-induced death[26]. AP002807.1 could enhance cellular resilience by regulating autophagy and cytoskeletal homeostasis[27,31]. Although AC005076.1 has not been extensively studied, its co-expression with SLC7A11 and MYH9 implies a potential role in redox balance and cytoskeletal regulation. L3MBTL4-AS1 may influence the tumor immune microenvironment via effects on macrophage populations, indirectly affecting AML progression and stress response[28]. Together, these insights highlight that the six lncRNAs are not only prognostic markers but may also actively participate in pathways critical to AML survival and disulfidptosis. Further experimental validation is warranted to elucidate their mechanistic roles.

To further investigate the biological pathways associated with disulfidptosis-related lncRNAs, functional annotation analysis was conducted. Given the complexity of cancer development process, GO functional analysis showed that lncRNAs associated with disulfidptosis are involved in cytokine binding, collagen-containing extracellular matrix, and negative regulation of immune system process. Within the tumor microenvironment (TME), the presence of Th2 (T helper type 2) cells can hinder the rejection of tumors induced by T cells. This occurs when Th2 cells produce cytokines such as IL-4 and IL-13, which stimulate the formation of immunosuppressive type 2-polarized macrophages (M2). This, in turn, promotes the growth and metastasis of tumors[32–34]. Additionally, excessive collagen in the extracellular matrix (ECM) leads to increased crosslinking, densification, and mechanical stress, which result in ECM stiffening[35]. This stiffening creates a favorable environment for tumor growth by impeding the function of cytotoxic $CD8^+$ T cells[36]. As a result, tumor cells are able to elude immune response even when $CD8^+$ T cells are stimulated. Furthermore, KEGG enrichment analysis showed that genes elevated in the high-risk group were primarily engaged in the chemokine signaling pathway, which plays a key role in maintaining the localization and function of hematopoietic stem and progenitor cells (HSPCs) in specific bone marrow microenvironment niches[37,38]. The over-activated chemokine signaling pathway may result in the accumulation of mutations in HSPCs in bone marrow, ultimately leading to the development of AML[39,40].

We also investigated the variations in the tumor immune microenvironment between the low-risk and high-risk groups, finding that immune-related components and cells were expressed differently in the two group. Interestingly, compared to the low-risk group, the high-risk group had noticeable greater levels of Tregs and monocytes. Tregs play multiple roles in immune suppression, and their abundance correlates with worse cancer outcomes[41]. Studies have shown that eliminating Treg cells can promote anti-tumor immunity and overcome immune unresponsiveness to syngeneic tumors. However, systemic depletion of Treg cells may also result in autoimmunity[42–44]. Similarly, high monocyte counts have been associated with an unfavorable prognosis in various types of cancer[45–47]. In vivo studies have observed that high monocyte counts can enhance tumor formation and angiogenesis while simultaneously suppressing the immune response against tumors[48]. These immune cell dynamics offer important therapeutic implications. The enrichment of Tregs and monocytes in the high-risk group suggests a highly immunosuppressive microenvironment, which may hinder effective anti-leukemic immune responses. Therapeutic strategies targeting immunosuppressive components, such as anti-CD25 monoclonal antibodies to deplete Tregs or CSF1R inhibitors to modulate myeloid-derived suppressor cells, could be particularly beneficial for these patients[49]. Furthermore, the upregulation of immune checkpoint pathways in high-risk individuals indicates that immune checkpoint blockade therapies, such as anti-PD-1 or anti-PD-L1 antibodies, might offer promising clinical benefits[50]. In contrast, low-risk patients, characterized by higher infiltration of effector immune cells like follicular helper T cells and γδ T cells, may respond more favorably to immune-stimulatory approaches, including IL-2 variants or CD137 agonists[51,52]. These findings highlight the potential utility of our lncRNA-based risk model not only in prognostication but also in guiding immunotherapy stratification for AML patients.

Moreover, our findings have practical implications for clinical management. The disulfidptosis-related lncRNA risk model could be utilized to stratify AML patients early in the disease course, enabling clinicians to tailor treatment intensity based on risk classification. High-risk patients identified by the model may benefit from more aggressive or combination therapeutic strategies, such as BCL-2 inhibitors combined with immune checkpoint blockade, whereas low-risk patients could be considered for targeted regimens or de-escalated therapies, reducing unnecessary toxicity. Furthermore, this model could assist in selecting patients for enrollment in clinical trials testing novel immunotherapies or metabolic interventions targeting oxidative stress and cytoskeletal vulnerabilities. Integration of our risk signature into clinical practice holds promise to optimize personalized treatment approaches and improve survival outcomes for AML patients.

Chemotherapy remains the cornerstone for AML treatment, but emerging targeted therapies are increasingly seen as potential alternatives. Numerous clinical trials are currently testing the effectiveness of combining chemotherapy with these targeted therapies. To assess the potential benefits of these combination therapies, we analyzed the sensitivity of drugs currently in clinical use and those undergoing clinical trials. Among the medications exhibiting increased sensitivity in the high-risk category were BCL-2 protein inhibitors, including obatoclax mesylate, venetoclax, and navitoclax. Obatoclax mesylate, an indole bipyrrole, imitates the BH3 domain. It prevents pro-apoptotic proteins from attaching itself to anti-apoptotic proteins' hydrophobic groove[53]. Venetoclax is a small-molecule BCL-2 homology domain 3–mimetic drug[54]. And navitoclax triggers apoptosis by activating caspase, permeabilizing the outer membrane of the mitochondria, producing proteins which promote apoptosis, and inhibiting targets that promote survival[55,56]. In the low-risk group, certain medications have shown to be more sensitive. These include pictilisib, dactolisib, GNE-317, vinblastine, and vinorelbine, which all contribute to the PI3K pathway and vinblastine analogues. Dactolisib, pictilisib, and GNE-317 are dual pan-PI3K/mTOR kinase inhibitors. It is believed that dactolisib and pictilisib have potential anti-neoplastic action due to their structural similarities between the ATP-binding region of PI3K's p110 subunit

and the catalytic domain of mTOR[57–59]. Additionally, GNE-317 is capable of crossing the blood-brain barrier[60]. Vinblastine analogues are antineoplastic drugs that target microtubule depolymerization, exhibiting antitumor effect[61]. Therefore, the observed differences in drug sensitivity suggest distinct mechanisms involving BCL-2 protein inhibition, PI3K/mTOR kinase inhibition, and interfering with microtubule assembly.

Despite the promising findings, our study has limitations that warrant further investigation. For instance, the validation of our model's accuracy was restricted to AML patients from the TCGA database. Although we fully recognize that validating the prognostic model using an independent external cohort would enhance its generalizability and clinical relevance, this remains a challenge due to the novelty of disulfidptosis-related lncRNAs. We conducted an extensive search in the GEO database for suitable RNA-seq datasets. However, we found that most commonly used platforms such as GPL96, GPL97, and GPL570 do not cover or only partially cover the six lncRNAs included in our model. As a result, no external cohort containing adequate expression data of our selected lncRNAs could be identified. Therefore, we relied on internal validation by randomly dividing the TCGA cohort into training and testing subsets, as shown in Fig. 4. While this internal validation supports the robustness of our model, we acknowledge that the absence of external validation remains an area that warrants further improvement, and we emphasize the necessity of future prospective clinical studies or high-quality external cohorts to confirm the predictive capacity of our lncRNA signature.

Moreover, the limited number of genes available in the GEO or TCGA databases hindered us from obtaining a suitable external cohort to validate our prognostic model. Furthermore, our immune cell infiltration analysis revealed that the high-risk group exhibited higher immune scores, which contrasts with observations in solid tumors, such as lung and colorectal cancers, where higher immune scores are often associated with improved survival. We hypothesize that this discrepancy may be due to the involvement of numerous AML-specific biological markers, including HLA-DR and CD37, in the calculation of the immune score, potentially influencing the observed results.

Conclusion

As a result, we created a predictive signature using lncRNAs associated with disulfidptosis. This signature has proven reliable in predicting prognosis, deciphering biological functions, and analyzing the immune infiltration landscape of AML. Furthermore, it holds potential for improving clinical prognostication, predicting chemotherapy sensitivity, and offers insights for future research on the interplay between disulfidptosis and acute myeloid leukemia.

Data availability

The authors declare that all data and materials supporting the findings of this article are available from the corresponding authors upon request.

Received: 19 February 2024; Accepted: 7 May 2025
Published online: 16 May 2025

References

1. SEER. Acute Myeloid Leukemia—Cancer Stat Facts. Available from: https://seer.cancer.gov/statfacts/html/amyl.html
2. Carter, B. Z. et al. Targeting MCL-1 dysregulates cell metabolism and leukemia-stroma interactions and resensitizes acute myeloid leukemia to BCL-2 Inhibition. *Haematologica* **107**(1), 58–76 (2022).
3. Janssen, M. et al. Venetoclax synergizes with gilteritinib in FLT3 wild-type high-risk acute myeloid leukemia by suppressing MCL-1. *Blood* **140**(24), 2594–2610 (2022).
4. Shallis, R. M., Bewersdorf, J. P., Boddu, P. C. & Zeidan, A. M. Hedgehog pathway inhibition as a therapeutic target in acute myeloid leukemia. *Expert Rev. Anticancer Ther.* **19**(8), 717–729 (2019).
5. Tangella, A. V., Gajre, A. & Kantheti, V. V. Isocitrate dehydrogenase 1 mutation and Ivosidenib in patients with acute myeloid leukemia: A comprehensive review. *Cureus* **15**(9), e44802 (2023).
6. Tallman, M. S. et al. Acute myeloid leukemia, version 3.2019, NCCN clinical practice guidelines in oncology. *J. Natl. Compr. Canc Netw.* **17**(6), 721–749 (2019).
7. Chen, L. L. & Carmichael, G. G. Long noncoding RNAs in mammalian cells: What, where, and why? *Wiley Interdiscip Rev. RNA*. **1**(1), 2–21 (2010).
8. Loewen, G., Jayawickramarajah, J., Zhuo, Y. & Shan, B. Functions of LncRNA HOTAIR in lung cancer. *J. Hematol. Oncol.* **7**, 90 (2014).
9. Ming, H., Li, B., Zhou, L., Goel, A. & Huang, C. Long non-coding RNAs and cancer metastasis: Molecular basis and therapeutic implications. *Biochim. Biophys. Acta Rev. Cancer* **1875**(2), 188519 (2021).
10. Nn, P. & Cb, J. Z. T. The hallmarks of cancer metabolism: Still emerging. *Cell Metabol.* **34**(3). https://pubmed.ncbi.nlm.nih.gov/35123658/ (2022),
11. Tong, X. et al. Targeting cell death pathways for cancer therapy: Recent developments in necroptosis, pyroptosis, ferroptosis, and cuproptosis research. *J. Hematol. Oncol.* **15**(1), 174 (2022).
12. Liu, X. et al. Actin cytoskeleton vulnerability to disulfide stress mediates disulfidptosis. *Nat. Cell. Biol.* **25**(3), 404–414 (2023).
13. Jaeger, N. et al. Single-cell analyses of Crohn's disease tissues reveal intestinal intraepithelial T cells heterogeneity and altered subset distributions. *Nat. Commun.* **12**, 1921 (2021).
14. Yoshihara, K. et al. Inferring tumour purity and stromal and immune cell admixture from expression data. *Nat. Commun.* **4**(1), 2612 (2013).
15. Chen, B., Khodadoust, M. S., Liu, C. L., Newman, A. M. & Alizadeh, A. A. Profiling tumor infiltrating immune cells with CIBERSORT. In *Cancer Systems Biology. Methods in Molecular Biology*, vol. 1711, 243–259 (eds. Von Stechow, L.) (Springer, 2018). http://link.springer.com/ (2018). https://doi.org/10.1007/978-1-4939-7493-1_12
16. Bindea, G. et al. Spatiotemporal dynamics of intratumoral immune cells reveal the immune landscape in human cancer. *Immunity* **39**(4), 782–795 (2013).
17. Short, N. J., Rytting, M. E. & Cortes, J. E. Acute myeloid leukaemia. *Lancet* **392**(10147), 593–606 (2018).
18. Papaemmanuil, E. et al. Genomic classification and prognosis in acute myeloid leukemia. *N. Engl. J. Med.* **374**(23), 2209–2221 (2016).

19. Feng, Z. H. et al. m6A-immune-related LncRNA prognostic signature for predicting immune landscape and prognosis of bladder cancer. *J. Transl Med.* **20**(1), 492 (2022).
20. Wu, Z. et al. Identification and validation of ferroptosis-related LncRNA signatures as a novel prognostic model for colon cancer. *Front. Immunol.* **12**, 783362 (2021).
21. Li, X. X. et al. Analysis of differential expressions of long non-coding RNAs in nasopharyngeal carcinoma using next-generation deep sequencing. *J. Cancer* **9**(11), 1943–1950 (2018).
22. Li et al. Identification of long noncoding RNAs as predictors of survival in triple-negative breast cancer based on network analysis. BioMed research international [Internet]. 2020 Mar 3 [cited 2024 Jan 20];2020. Available from: https://pubmed.ncbi.nlm.nih.gov/32190687/
23. Li, N. et al. LncRNA THAP9-AS1 promotes pancreatic ductal adenocarcinoma growth and leads to a poor clinical outcome via a sponging miR-484 and interacting with YAP. *Clin. Cancer Res.* **26**(7), 1736–1748 (2020).
24. Jia, W. et al. Long noncoding RNA THAP9-AS1 is induced by *Helicobacter pylori* and promotes cell growth and migration of gastric cancer. *Onco Targets Ther.* **12**, 6653–6663 (2019).
25. Pan, J. & Zhao, L. Long non-coding RNA histone deacetylase 4 antisense RNA 1 (HDAC4-AS1) inhibits HDAC4 expression in human ARPE-19 cells with hypoxic stress. *Bioengineered* **12**(1), 2228–2237 (2021).
26. Liu, L. et al. Knockdown of LINC01694 inhibits growth of gallbladder cancer cells via miR-340-5p/Sox4. *Biosci. Rep.* **40**(4), BSR20194444 (2020).
27. Li, X. et al. A novel prognostic model based on autophagy-related long non-coding RNAs for clear cell renal cell carcinoma. *Front. Oncol.* **11**, 711736 (2021).
28. Bajpai, G. et al. The human heart contains distinct macrophage subsets with divergent origins and functions. *Nat. Med.* **24**(8), 1234–1245 (2018).
29. Li, N. et al. LncRNA *THAP9-AS1* promotes pancreatic ductal adenocarcinoma growth and leads to a poor clinical outcome via sponging miR-484 and interacting with YAP. *Clin. Cancer Res.* **26**(7), 1736–1748 (2020).
30. Du, J., Ji, Q., Dong, L., Wang, L. & Xin, G. HDAC4-AS1/CTCF transcriptionally represses HDAC4 under stress, whereas HDAC4 inhibits stress-induced syncytiotrophoblast cellular pyroptosis by deacetylating NLRP3 and GSDMD. *Cell. Biochem. Function* **43**(3), e70064 (2025).
31. Pan, J. et al. Identification of a cancer driver gene-associated LncRNA signature for prognostic prediction and immune response evaluation in clear cell renal cell carcinoma. *Transl Cancer Res.* **13**(7), 3418–3436 (2024).
32. Coussens, L. M., Zitvogel, L. & Palucka, A. K. Neutralizing tumor-promoting chronic inflammation: A magic bullet? *Science* **339**(6117), 286–291 (2013).
33. Santoni, M. et al. Emerging role of tumor-associated macrophages as therapeutic targets in patients with metastatic renal cell carcinoma. *Cancer Immunol. Immunother.* **62**(12), 1757–1768 (2013).
34. Zhao, G. et al. Activation of epidermal growth factor receptor in macrophages mediates feedback Inhibition of M2 polarization and Gastrointestinal tumor cell growth. *J. Biol. Chem.* **291**(39), 20462–20472 (2016).
35. Sun, B. The mechanics of fibrillar collagen extracellular matrix. *Cell. Rep. Phys. Sci.* **2**(8), 100515 (2021).
36. Cohen, I. J. & Blasberg, R. Impact of the tumor microenvironment on tumor-Infiltrating lymphocytes: Focus on breast Cancer. *Breast Cancer (Auckl)* **11**, 1178223417731565 (2017).
37. Greenbaum, A. et al. CXCL12 in early mesenchymal progenitors is required for haematopoietic stem-cell maintenance. *Nature* **495**(7440), 227–230 (2013).
38. Ding, L. & Morrison, S. J. Haematopoietic stem cells and early lymphoid progenitors occupy distinct bone marrow niches. *Nature* **495**(7440), 231–235 (2013).
39. Hanekamp, D., Cloos, J. & Schuurhuis, G. J. Leukemic stem cells: Identification and clinical application. *Int. J. Hematol.* **105**(5), 549–557 (2017).
40. Chopra, M. & Bohlander, S. K. The cell of origin and the leukemia stem cell in acute myeloid leukemia. *Genes Chromosomes Cancer* **58**(12), 850–858 (2019).
41. Shang, B., Liu, Y., Jiang, S. & juan, Liu, Y. Prognostic value of tumor-infiltrating FoxP3 + regulatory T cells in cancers: A systematic review and meta-analysis. *Sci. Rep.* **5**, 15179 (2015).
42. Shimizu, J., Yamazaki, S. & Sakaguchi, S. Induction of tumor immunity by removing CD25 + CD4 + T cells: A common basis between tumor immunity and autoimmunity. *J. Immunol.* **163**(10), 5211–5218 (1999).
43. Onizuka, S. et al. Tumor rejection by in vivo administration of anti-CD25 (interleukin-2 receptor alpha) monoclonal antibody. *Cancer Res.* **59**(13), 3128–3133 (1999).
44. Yamaguchi, T. & Sakaguchi, S. Regulatory T cells in immune surveillance and treatment of cancer. *Semin Cancer Biol.* **16**(2), 115–123 (2006).
45. Shigeta, K. et al. High absolute monocyte count predicts poor clinical outcome in patients with castration-resistant prostate cancer treated with docetaxel chemotherapy. *Ann. Surg. Oncol.* **23**(12), 4115–4122 (2016).
46. Lee, Y. Y. et al. Prognostic value of pre-treatment circulating monocyte count in patients with cervical cancer: Comparison with SCC-Ag level. *Gynecol. Oncol.* **124**(1), 92–97 (2012).
47. Sasaki, A. et al. Prognostic value of preoperative peripheral blood monocyte count in patients with hepatocellular carcinoma. *Surgery* **139**(6), 755–764 (2006).
48. Boros, P., Ochando, J. C., Chen, S. H. & Bromberg, J. S. Myeloid-derived suppressor cells: Natural regulators for transplant tolerance. *Hum. Immunol.* **71**(11), 1061–1066 (2010).
49. Solomon, I. et al. CD25-Treg-depleting antibodies preserving IL-2 signaling on effector T cells enhance effector activation and antitumor immunity. *Nat. Cancer* **1**(12), 1153–1166 (2020).
50. Li, W., Wang, F., Guo, R., Bian, Z. & Song, Y. Targeting macrophages in hematological malignancies: Recent advances and future directions. *J. Hematol. Oncol.* **15**(1), 110 (2022).
51. Faliti, C. E. et al. Interleukin-2-secreting T helper cells promote extra-follicular B cell maturation via intrinsic regulation of a B cell mTOR-AKT-Blimp-1 axis. *Immunity* **57**(12), 2772–2789e8 (2024).
52. Malyshkina, A. et al. Immunotherapy-induced cytotoxic T follicular helper cells reduce numbers of retrovirus-infected reservoir cells in B cell follicles. *PLoS Pathog.* **19**(10), e1011725 (2023).
53. Joudeh, J. & Claxton, D. Obatoclax mesylate: Pharmacology and potential for therapy of hematological neoplasms. *Expert Opin. Investig. Drugs* **21**(3), 363–373 (2012).
54. Guièze, R. et al. Mitochondrial reprogramming underlies resistance to BCL-2 Inhibition in lymphoid malignancies. *Cancer Cell.* **36**(4), 369–384e13 (2019).
55. Souers, A. J. et al. ABT-199, a potent and selective BCL-2 inhibitor, achieves antitumor activity while sparing platelets. *Nat. Med.* **19**(2), 202–208 (2013).
56. Tse, C. et al. ABT-263: a potent and orally bioavailable Bcl-2 family inhibitor. *Cancer Res.* **68**(9), 3421–3428 (2008).
57. Rodon, J., Dienstmann, R., Serra, V. & Tabernero, J. Development of PI3K inhibitors: Lessons learned from early clinical trials. *Nat. Rev. Clin. Oncol.* **10**(3), 143–153 (2013).
58. Folkes, A. J. et al. The identification of 2-(1H-indazol-4-yl)-6-(4-methanesulfonyl-piperazin-1-ylmethyl)-4-morpholin-4-yl-thieno[3,2-d]pyrimidine (GDC-0941) as a potent, selective, orally bioavailable inhibitor of class I PI3 kinase for the treatment of cancer. *J. Med. Chem.* **51**(18), 5522–5532 (2008).

59. Foukas, L. C. et al. Critical role for the p110alpha phosphoinositide-3-OH kinase in growth and metabolic regulation. *Nature* **441**(7091), 366–370 (2006).
60. Heffron, T. P. et al. The design and identification of brain penetrant inhibitors of phosphoinositide 3-kinase α. *J. Med. Chem.* **55**(18), 8007–8020 (2012).
61. Wang, Y. N. et al. Vinblastine resets tumor-associated macrophages toward M1 phenotype and promotes antitumor immune response. *J. Immunother. Cancer* **11**(8), e007253 (2023).

Author contributions
Professor Daoxin Ma designed and funded the research. Yihong Wei performed the research. Hexiao Jia helped design the research and wrote the manuscript. Xiaodong Guo and Hailei Zhang assisted with the research. He Na and Can Can analyzed the data. Hanyang Wu, Xinyu Yang and Wancheng Liu edited the paper.

Funding
This work was supported by the National Natural Science Foundation of China (grant numbers: No.82370173, No. 32241005).

Declarations

Ethics approval and consent to participate
Our study was approved by the Medical Ethical Committee of Qilu Hospital of Shandong University (KYLL-2018-137) and informed consent was obtained from all participants. All methods were performed in accordance with the relevant guidelines. The research participants have been performed in accordance with the Declaration of Helsinki. And our study did not include any interventional clinical trial.

Consent for publication
All the authors agree to the content of the paper.

Competing interests
The authors declare no competing interests.

Additional information
Supplementary Information The online version contains supplementary material available at https://doi.org/10.1038/s41598-025-01730-8.

Correspondence and requests for materials should be addressed to D.M.

Reprints and permissions information is available at www.nature.com/reprints.

Publisher's note Springer Nature remains neutral with regard to jurisdictional claims in published maps and institutional affiliations.